Structural Characteristics of Gap Junctions. I. Channel Number in Coupled and Uncoupled Conditions

G. Zampighi, M. Kreman, F. Ramón,* A. L. Moreno,* and S. A. Simon‡

Department of Anatomy, Jerry Lewis Neuromuscular Research Center, UCLA School of Medicine, Los Angeles, California 90024; *Departamento de Fisiologia y Biofisica, Centro de Investigacion, Apartado Postal 14-740, Mexico, D. F. 07000, Mexico; and ‡Departments of Physiology and Anesthesiology, Duke University Medical Center, Durham, North Carolina 27710

Abstract. Gap junctions between crayfish lateral axons were studied by combining anatomical and electrophysiological measurements to determine structural changes associated during uncoupling by axoplasmic acidification. In basal conditions, the junctional resistance, R_j, was ~60–80 kΩ and the synapses appeared as two adhering membranes; 18–20-nm overall thickness, containing transverse densities (channels) spanning both membranes and the narrow extracellular gap (4–6 nm). In freeze-fracture replicas, the synapses contained $>3 \times 10^3$ gap junction plaques having a total of $\sim 3.5 \times 10^5$ intramembrane particles. "Single" gap junction particles represented ~10% of the total number of gap junction particles present in the synapse. Therefore, in basal conditions, most of the gap junction particles were organized in plaques. Moreover, correlations of the total number of gap junction particles with R_j suggested that most of the junctional particles in plaques corresponded to conducting channels.

Upon acidification of the axoplasm to pH 6.7–6.8, the junctional resistance increased to ~300 kΩ and action potentials failed to propagate across the septum. Morphological measurements showed that the total number of gap junction particles in plaques decreased ~11-fold to 3.1×10^4 whereas the number of single particles dispersed in the axolemmae increased significantly. Thin sections of these synapses showed that the width of the extracellular gap increased from 4–6 nm in basal conditions to 10–20 nm under conditions where axoplasmic pH was 6.7–6.8. These observations suggest that single gap junction particles dispersed in the synapse most likely represent hemi-channels produced by the dissasembly of channels previously arranged in plaques.

Gap junctions are specialized regions of contact between the plasma membranes of most cells. They consist of plaques of channels which span both plasma membranes and bridge the narrow intervening extracellular gap (2, 34, 38). Most gap junction channels are dodecamers comprised of two opposing hexamers linked together through their extracellular domains (20, 21, 48–50, 55, 56, 59). Functionally, gap junction channels provide an aqueous pathway for the passage of cations and small molecules between cell cytoplasms. Single channel recordings have demonstrated that gap junction channels appear to behave as independent units exhibiting both open and closed states (4, 24, 51). Therefore, the junctional conductance (g_j; the electrical parameter used to quantify the easiness with which the junction permits transfer of ions and/or charged molecules between cells) is equal to the product of the single channel conductance (δ_j) times the mean number of open channels (n_o) (i.e., $g_j = \delta_j \times n_o$). Changes in g_j can be the result of changes in the single channel conductance (δ_j), the ratio of open to closed (n_c) channels (n_o/n_c), or the total number of channels ($n_t = n_o + n_c$). Experimental procedures that lead to changes in g_j such as changes in transjunctional or transmembrane voltages (25, 43, 44) increasing the intracellular H^+ (42, 45, 46, 47) or Ca^{++} (18, 19, 39) concentrations, application of calmodulin inhibitors (29, 30), the local anesthetics heptanol and octanol (13), second messengers such as cAMP (10, 5, 16, 40), and diacylglycerol (53), can be explained by any of the three mechanisms listed above. To distinguish between these three mechanisms one needs measurements of g_j and δ_j and an independent measurement of the total number of gap junction channels, n_t.

To measure n_t, we have taken advantage of the special structural and physiological characteristics of the synapses between the lateral giant axons of the crayfish. Electrophysiological studies provide values of g_j both in basal conditions (12) and at which action potentials fail to propagate across the septa (uncoupled). This means that uncoupling in crayfish lateral axons has both a well-defined endpoint and a precise physiological interpretation (14). Structurally, crayfish lateral axons have several advantages that enable one to measure n_t. First, gap junction plaques are located in septa of distinct morphology rather than scat-

© The Rockefeller University Press, 0021-9525/88/05/1667/12 $2.00

tered throughout the cell surface as in most cells (8, 9, 26–28, 31, 35–37, 54). Second, in freeze-fracture replicas, the channels appear as ~12-nm-diam intramembrane particles located on the E-face, the fracture face with fewer particles (6, 9, 28). The particular location and diameter make the particles that are not organized in plaques readily distinguishable from regular nonjunctional particles (of ~8 nm diam). Thus, in crayfish lateral axons, n_t (i.e., particles organized in plaques and single particles) can be quantified, and by correlating these number to measurements of g_j, a hypothesis of the mechanism(s) used by cells to uncouple gap junctions can be formulated.

The results in this paper suggest (*a*) in basal conditions, ~90% of the gap junction particles are organized in plaques ($n_t \approx n_p$); (*b*) plaques are comprised predominantly of open channels ($n_p \approx n_o$); (*c*) uncoupling by acidification decreases the number of particles in plaques (n_p) by ~11-fold which can account for the decrease in g_j; and, (*d*) the single gap junction particles dispersed into the axolemmae upon uncoupling most likely correspond to hemichannels resulting from the disassembly of the channels previously aggregated in plaques.

Materials and Methods

Animals and Solutions

Experiments were performed on adult crayfish (*Procambarus clarkii*) of either sex obtained from Western Scientific (Sacramento, CA) or through a local supplier in Mexico City. The animals were maintained in well-oxygenated tanks for up to 2–3 wk. Crayfish about to molt were not used in these studies. All animals were sacrificed at 9 a.m. to avoid the normal variations in the sensitivity of the gap junctions to acidification during a 24-h cycle (23). Animals were sacrificed and their abdominal ventral cords were excised and placed in a dish containing a modified van Harreveld (VH)[1] solution of the following composition: 205 mM NaCl, 5 mM KCl, 13.5 mM $CaCl_2$, and 5 mM Hepes, pH 7.4. Increases in junctional resistance (R_j) were produced by replacing totally (205 mM) or partially (50 mM) the NaCl in the VH solution with Na acetate. Na acetate in the external solution decreases the intracellular pH (pH_i) because acetate diffuses across the membrane and it dissociates in the axoplasm into a proton and an acetate anion. All VH solutions were adjusted to pH 7.4.

Anatomical experiments were performed in nerve cords exposed to VH solution (basal conditioins) or to solutions in which 50 mM of the NaCl was replaced with 50 mM Na acetate. The second and third abdominal ganglia of over 100 animals were used in this study.

Electrophysiological Measurements

Nerve cords were desheathed and the lateral axons at the level of the third abdominal ganglium were impaled with four microelectrodes, two on each side of the septum, as described previously (32). Rectangular pulses of 100 nA were injected alternately into each axon with two electrodes while transmembrane voltages (V_1, V_1^*, V_2, V_2^*) were measured with the two other electrodes. The junctional and input resistances to each axon were calculated from these voltages' responses, as described previously by Watanabe and Grundfest (52). Briefly, V_1 and V_2 are the recorded transmembrane voltages from both axons after injection of current I_1, and V_1^* and V_2^* are those when current I_2 is injected. Junctional resistance (R_j) was calculated from these voltage and current values by substituting in the equations describing the equivalent circuit of two coupled axons (see Fig. 1).

In five experiments, pH_i was measured with pH-sensitive glass microelectrodes inserted in one of the axons as described previously (23). These microelectrodes were silanized, filled with a liquid ionic exchange resin (Fluka 82500) and backfilled with 100 mM trisodium citrate dihydrate and 100 mM NaCl adjusted to pH 6.0. All microelectrodes were calibrated before and after the experiments and those with a slope <55 mV per decade were rejected.

1. *Abbreviation used in this paper*: VH, van Harreveld.

Electron Microscopy

Fixation. Crayfish abdominal cords were fixed as described previously (55, 57). Briefly, the abdominal nerve cords were successively fixed in (*a*) 3% glutaraldehyde-H_2O_2 in 0.2 M Na cacodylate at pH 7.3 for 30 min in the dark; (*b*) 3% glutaraldehyde in 0.2 M Na cacodylate buffer for 30 min; and (*c*) 3% glutaraldehyde in 0.2 M Na cacodylate buffer containing 0.3–0.5% tannic acid for 1 h. After fixation the nerve cords were washed in 0.1 M Na cacodylate buffer containing 4% sucrose. Postfixation was carried out in 2% osmium tetroxide in 0.1 M Na cacodylate buffer for 90 min at room temperature. The cords were wased in 0.1 M Na acetate, pH 5.2, and stained en bloc with 0.5% uranyl acetate in 0.1 M Na acetate at 5°C for 12 h. Dehydration was performed in ethanol, and infiltration and embedding were performed in Epon 812.

Sectioning. Thick sections of the septal region were cut both perpendicular and parallel to the long axis of the axons. When sectioned perpendicularly, the ganglia were oriented in the block such that the septum was always sectioned in the rostral-to-caudal direction. Two complete septa from different animals were serially sectioned (section thickness: 1–2 μm) to determine their size, shape, and number of synaptic regions. These sections were collected on glass slides stained with toluidine blue.

Thin sections were cut with a diamond knife on an ultramicrotome (Sorvall MT-5,000; DuPont Co., Wilmington, DE). Sections having gray interference colors were mounted on formvar-coated single hole grids stabilized with carbon, double stained with 2% uranyl acetate dissolved in water for 10 min, and lead citrate solutions for 3–5 min. In all the ganglia, thin sections were collected first from the rostral portion of the septum and later from the more caudal portions. In each septum, ribbons of thin sections were obtained from a minimum of five different synaptic areas. Observations were made with an electron microscope (Zeiss EM-IDC; Carl Zeiss, Inc., Thornwood, NY) at 80 kV.

Freeze-fracture. For the freeze-fracture experiments, nerve cords were fixed using the fixation procedure described above (except that step *c* was omitted). To increase the probability that the fracture plane passed through the septum, regions containing only septa were excised from the ganglia. These isolated septal regions were first immersed in 10% glycerol in 0.2 M Na cacodylate buffer, pH 7.3, and then in 25% glycerol prepared in the same buffer. The pieces were placed on standard holders (Balzers, Hudson, NH) and plunged into liquid propane cooled to −190°C in a liquid nitrogen bath. Freeze-fracture was performed in a Balzers 400K at −150°C and at a vacuum of 10^{-7} mbar. Fracturing was done with a knife cooled to liquid nitrogen temperature. The flat fractured surface was shadowed unidirectionally by evaporating Pt-C at 45°C immediately after the last pass of the cold knife. Also, several fractured septa were rotary shadowed at 25°C using a cryogenic rotary cold stage model TSR-1004D at 250 rpm (Wiltek Industries LTD., Bedford, NH). Carbon was evaporated at 90°C.

The following technique was used to prevent fragmentation of the replicas which complicates the collection of the data for quantitative analysis. The fractured specimens were covered with a drop of 0.5% collodion in amyl acetate while still frozen. The excess collodion was removed and the thin remaining layer of plastic was allowed to dry. This layer of plastic maintained the replica as a whole during the subsequent digestion and washes. The tissue was digested for 30 min in 5.25% Na hypochlorite (Purex bleach) and the entire collodion-coated replica was released from the tissue in a single piece. The replicas were then washed by transferring them to three successive distilled water baths, ~10 min each. The plastic-coated replica was picked up from below using a formvar-coated single hole grid (hole size 1 × 2 mm) and allowed to dry. The collodion was subsequently removed by immersing the grid in amyl acetate for ~30 s. Therefore, in this study, each replica represents a different septa.

Quantification of the Electron Microscopic Observations

Septum. The shape of the septum is approximately elliptical. Its surface area (*As*) was calculated from the equation $As = \pi ab/4$, where *a* and *b* are the major and minor axes, respectively. The lengths of the two axes were obtained from thick serial sections. The major axis, oriented obliquely with respect to the long axis of the axon, was obtained by multiplying the total number of thick sections that contained septa by the section thickness. The minor axis corresponds to the diameter of the axons at the region of the septum. This measurement was obtained by digitizing the length of the septum in each one of the thick sections with a computer-aided morphometric system consisting of an IBM-AT computer driven by an AUTOCAD (Autodesk, Inc., Sausalito, CA) software package. The total septal area provided an idea of the area of freeze-fracture replicas of the septum to be studied in axons fixed in both basal and uncoupled conditions.

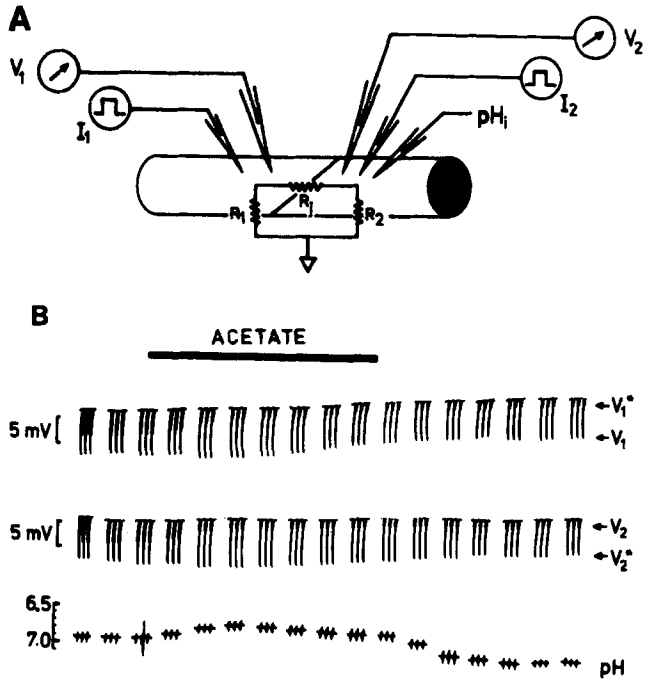

Figure 1. (*A*) Diagram of the experimental set up indicating the position of the microelectrodes. Superimposed is the equivalent circuit. (*B*) Voltage (*upper traces*) and internal pH (*lower traces*) responses when 0.05 M NaCl in the VH solution was replaced by 0.05 M Na acetate (*bar*). The upper traces represent the voltage response of both axons (*1* and *2*) to current pulses of 100 nA applied alternately to each axon. The records show groups of three pulses applied to each axon every 5 min. The progressive decrease in the amplitudes of V_2 and V_1* is indicative of the increase in R_j. The lower trace is a pH_i recording from an internal electrode in one of the axons. It contains small artifacts due to incomplete subtraction of voltage between the voltage and pH amplifiers. The bar at the top indicates the duration of the Na acetate application.

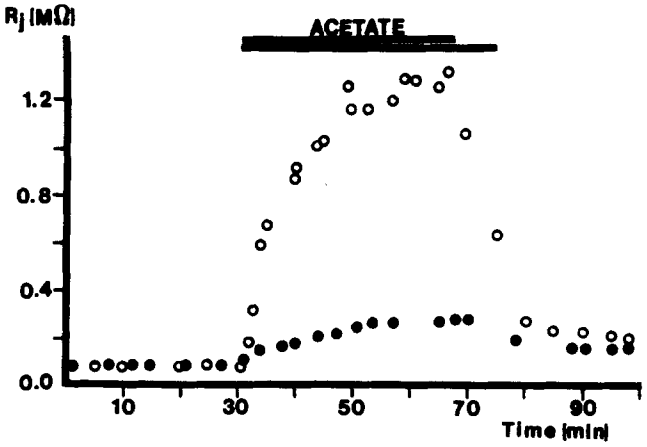

Figure 2. Plots of junctional resistance R_j vs. time during substitution of 0.205 (○) and 0.05 M (●) NaCl for Na acetate solutions. R_j values were calculated from voltage records of the type shown in Fig. 1. In the presence of 0.205 M Na acetate, R_j increased from its basal value of ~80 kΩ to 1.2 MΩ in 20–25 min. In the presence of 0.05 M Na acetate, R_j increased from 80 to ~320 kΩ in 20–25 min and action potentials failed to propagate across the septa. Replacement of the acetate solutions with VH showed that the process is reversible.

Synapse. The synaptic area (region of axolemmal contact) was measured in freeze-fracture replicas covering extensive areas of septum (see Fig. 5 *A*). Of the >100 freeze-fracture experiments performed in this study, only 16 (7 from axons basal conditions and 9 from uncoupled axons) were used. Each replica represented a different septa. All the quantifications were performed on E-faces because that is the fracture face in which gap junction particles are located in arthropods (6, 28). Low magnification images (either 7,500× or 15,000×) of large septal areas (each one of >2,000 μm²) were used to assemble montages such as the one shown in Fig. 5 *A*. The areas and perimeters of both synaptic regions and gap junction plaques were measured using the computer-aided morphometric system.

Gap Junctional Plaques. The area of gap junction plaques (A_{gj}) was measured in >1,500 μm² of synapse for each case. The number of particles aggregated in plaques, n_p, was calculated by assuming that the particles formed a two-dimensional hexagonal crystal from the equation: $n_p = \beta A_{gj}/A_{ch}$. The correction factor, β, accounts for the fractional area of the unit cell (the basic building of the hexagonal crystal which repeats infinitely in two dimensions) that does not contain channels and A_{ch} is the area occupied by a single channel. A_{ch} was calculated from the diameter of the intramembrane particles in the patches measured in freeze-fracture replicas of specimens unidirectionally and rotary shadowed. β was obtained from the ratio A_{ch}/A_{uc}, where A_{uc} is the unit cell area estimated from the center-to-center distance between particles (D [19.5 ± 1.6 nm; mean ± SD; n = 26]), measured by optical diffraction using the equation $A_{uc} = D^2 \cos 30°$. This method of area integration has an error of ~5%, as estimated by counting the exact number of particles by eye and comparing the counted number with the number calculated from the gap junction area. Plaques containing up to 10 particles were counted by eye. Thus the first bar of the histogram in Fig. 6 is an exact number. Plaques were defined as clusters of 12-nm-diam particles spaced ~20 nm apart. Clusters of six particles were the smallest units to fit this definition.

Plaque Particle–Single Particle Ratio. The ratio of particles contained in plaques to single gap junction particles was estimated from micrographs enlarged to 120,000× (final magnification). The diameter of the gap junctional particles (12.1 ± 0.9 nm, mean ± SD; n = 40) was measured from 25,000× and 40,000× negatives using a Nikon Profile Projector model 6C (Nikon Inc., Garden City, NY). Single gap junction particles were distinguished from regular intramembrane particles (8.0 ± 0.1 nm diam, mean ± SD; n = 72) on the basis of their diameter and location on the E-faces. In septa uncoupled by axoplasmic acidification, the number of single junctional particles greatly increased. No quantification was performed in this condition because the particles were spread over much larger areas of the septum and sampling of such large areas was beyond the scope of this study.

Results

Electrophysiology

Fig. 1 shows the voltage responses of both axons to rectangular current pulses of 100 nA injected alternately in each axon. These traces are labeled V_1*, V_1 (upper) and V_2, V_2* (lower) as described in Materials and Methods. The traces at the extreme left side show the relative magnitudes of the voltages of the axons in basal conditions bathed in VH solution. At the time indicated by the bar, 0.05 M NaCl of the VH solution was replaced by 0.05 M Na acetate. After a few minutes, uncoupling was observed as a progressive decrease in the ratios of V_1^*/V_1 and V_2^*/V_2. The lower trace shows a recording of the intracellular pH (pH_i) for the same preparation described above. In basal conditions, pH_i remained constant at a value of ~7.0 whereupon it decreased to pH_i 6.7–6.8 when the axons were uncoupled by the substitution of 0.05 M NaCl for 0.05 M Na acetate in the VH solution. Upon removal of the acetate, pH_i recovered with a small overshoot.

Fig. 2 shows a plot of R_j against time obtained from two experiments in which two different acetate concentrations were applied for the time indicated by the bars. In one case (*open circles*) 0.205 M NaCl in the VH solution was replaced with 0.205 M Na acetate, while in the other (*filled circles*)

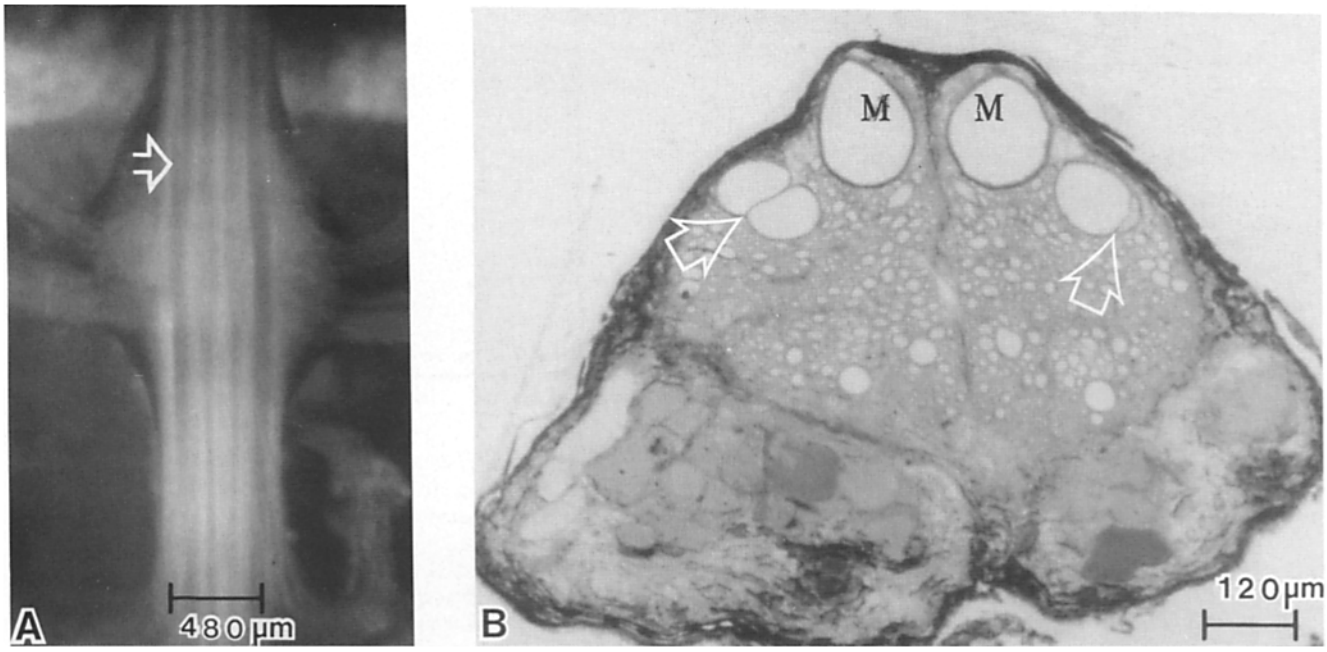

Figure 3. (*A*) Dorsal view of a crayfish nerve cord in situ at the level of the second abdominal ganglion (*rostral at top*). In this animal, the abdominal aorta was perfused with VH solution containing methylene blue. The four giant axons are seen as dark bands extending longitudinally throughout the entire cord. The left lateral axon has a diagonal line that extends from rostral to caudal and from lateral to medial directions. This line (*arrow*) corresponds to the septum. (*B*) Cross section of a third abdominal ganglion (*dorsal at top*). The darkly stained band surrounding the entire ganglion is the perineurium. The four giant axons were located immediately below the dorsal perineurium. The median giants were labeled *M* and the lateral giants are located laterally to these. The arrows point to the location of the septa in this cross section.

only 50 mM of NaCl was replaced. Complete replacement of NaCl induced a rapid increase in R_j to ~1.3 MΩ in 20 min, whereas replacement of 0.05 M of NaCl with 0.05 M Na acetate increased R_j to ~300 kΩ. In basal conditions, the nonjunctional resistances were ~100–150 kΩ. They did not change appreciably upon replacement of 0.05 M NaCl for Na acetate. However, they increased to ~200–250 kΩ during complete replacement of NaCl for Na acetate.

When the VH solution containing Na acetate was replaced by normal VH, R_j decreased to ~200 kΩ, a resistance significantly higher than the one recorded in basal conditions (80 kΩ). Recovery to basal values of R_j was obtained by washing the cords for longer times in VH (3).

Of the two acetate treatments described in Fig. 2, quantifications of the total number of gap junction particles were performed in axons uncoupled by replacement of 50 mM NaCl with 50 mM Na acetate (*filled circles*, Fig. 2). An advantage of this procedure was that R_j increased to relatively constant value (250–400 kΩ) over the same period of time (20–25 min). Within this range of R_j action potentials did not propagate across the septa.

Anatomy of the Septum

The abdominal portion of the crayfish nerve cord consists of six ganglia connected through interganglionic segments (11). When viewed dorsally, the cord displays two pairs of giant axons (Fig. 3, *A* and *B*) extending along its entire length. The pair closest to the midline are the medial giants and the ones placed laterally are the lateral giants. At the rostral third of each ganglion (*arrow*, Fig. 3 *A*), the lateral giants are interrupted by an oblique line oriented from rostral to caudal and from lateral to medial. This line is called the septum (11).

Fig. 3 *B* shows a cross section from the rostral portion of the third abdominal ganglion. The medial giants (*M*) have a smooth circular profile whereas the lateral giants are comprised of two profiles (the anterior and posterior segments) separated by septa (*arrows* in Fig. 3 *B*). Thick serial sections of two ganglia demonstrated that the septal region had an elliptical shape (*a/b* ratio of 4:1) and an area of ~2–3 × 10^4 μm².

Structural Characteristic of Synapses Fixed in Basal Conditions

The septum separating the segments of the lateral axons appeared in thin sections as a 1.5–2-μm-thick wall constructed of laminae of extracellular material covered by thin, interdigitating slabs of glial cells (*E* and *G* in Fig. 4). The septum also contained interruptions where the axolemmae of the two axons come into close apposition. These specialized regions are called synapses (Fig. 4, *arrows*) and correspond to the places where the two axons became in direct contact.

Synapses occupied extensive regions of the septa. Fig. 5 *A* shows a montage of a freeze-fracture replica which represents >7,000 μm² of the E-face of a septum (area between dark lines). The synapses (shown as blackened areas) occupied 6–7% of the septal area (or 1.35 ± 0.4 × 10^3 μm² mean ± SD; n = 7; Table I). The synaptic region enclosed in the rectangle and indicated by the arrow is presented at higher magnification in Fig. 5 *B*. The E-fracture face of this synapse was comprised of numerous gap junction plaques

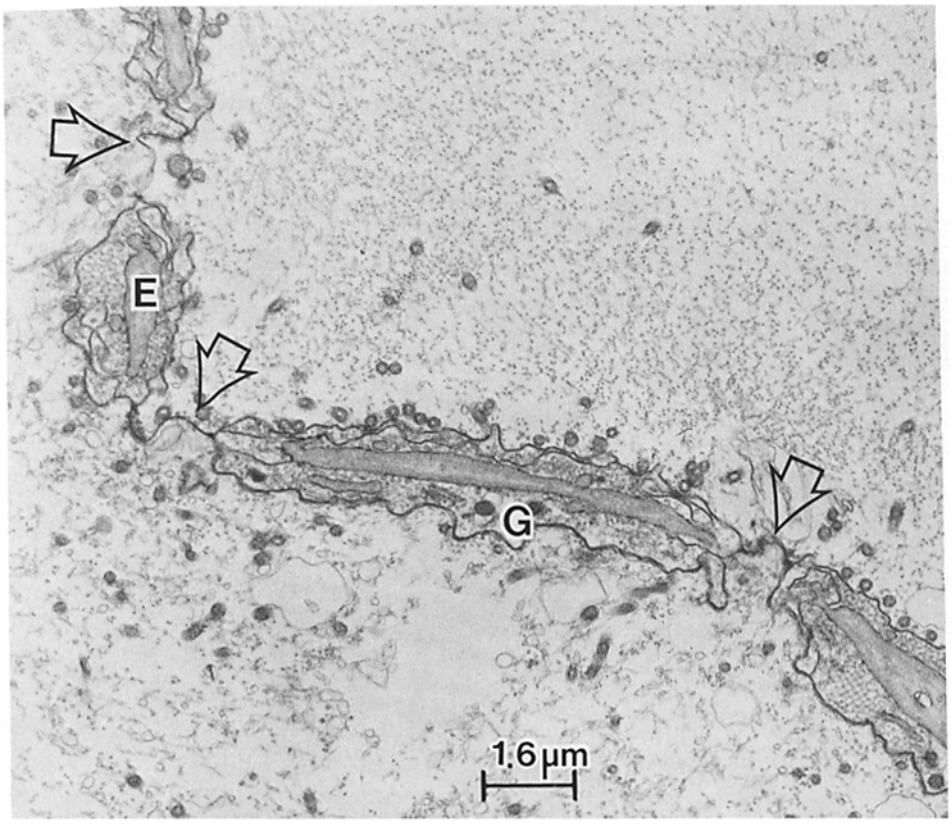

Figure 4. Transverse section of the septal region between anterior (*above*) and posterior segments of the lateral giant axons. The septum was constructed of laminae (*E*) of amorphous and fibrillar extracellular material surrounded by projections of glial cells (*G*) and interruptions (the synapses) at those regions where the axolemmae became in direct contact (*arrows*). The arrows point to interruptions of the septum where the axolemmae are in direct contact (the synaptic regions).

and nonjunctional axolemma (the smooth regions of the E-face). Gap junction plaques contained 12 ± 0.9-nm-diam intramembrane particles (mean ± SD; $n = 40$) located on the E-face with complementary pits on the P-face (*inset*, Fig. 5 *B*). The gap junction particles and their complementary pits on the P-face were spaced ~20 nm center to center (19.6 ± 1.6 nm, mean ± SD; $n = 23$) and occupied 8–10% of synaptic area (Table I). This fracture pattern displaying particles in the E-face and pits in the P-face is the reverse of that described for mammalian gap junctions (21), but characteristic of the junctions of insects and crustaceans (6, 9, 28, 31).

Septa fixed in basal conditions contained over 3,000 gap junction plaques of different sizes, occupying 0.4–0.7% of the area of the septum (Table I). Loosely packed aggregates containing 2–5 junctional particles were seldom observed. These small aggregates were not included in the quantifications of particles in plaques or "single" (see Materials and Methods). Fig. 6 shows a histogram of the distribution of the number of particles per plaque. The histogram shows that ~45% of the plaques contained from 6 to 30 particles. Although these small gap junction plaques were very numerous, they contained ~12% of the total number of gap junction particles. Thus, the omission of loose aggregates comprised of 2–5 particles does not introduce a significant error in the total number of particles (n_t) in basal conditions. In addition, single gap junction particles (defined as 12-nm-diam particles with a small deposit of metal at the center) represented ~10% of n_t. Therefore, the total number of gap junction particles in the synapse was approximately equal to the number of particles forming plaques (i.e., $n_t \approx n_p$).

Transverse thin sections of axons fixed under basal conditions demonstrated that the axolemmae were in close apposition over most of the synaptic region (Fig. 7 *A*). The gap junctional regions were comprised of two axolemmae separated by a small, unstained, 4–6-nm-wide extracellular gap (Fig. 7 *B*). In transverse sections, densities ~12 nm in diam and spaced ~20 nm apart, spanned the axolemmae and the extracellular gap, and protruded 2–3 nm into the axoplasm. All these structural characteristics distinguish the gap junctions of crayfish from those between mammalian tissues.

A striking feature of crayfish lateral giant axon gap junctions is the presence of 50–70-nm-diam vesicles associated with the junctional axolemmae (8, 9, 26–28, 31, 35–37, 59) (Fig. 7, *A* and *B*). Serial thin sections suggested that these vesicles were attached exclusively to the cytoplasmic surfaces of the synaptic regions and absent from the rest of the septa. Frequently, the vesicles were separated from the axolemma by clear spaces 7–10 nm wide. Occasionally, these vesicles were seen adhering (Fig. 7 *B*) or fusing (Fig. 8, *A* and *C*) with the axolemmae. The axoplasm of the synaptic region also contained large membrane-bound vacuoles with clear lumens and, infrequently, some tubular profiles (Fig. 7 *A*).

Structural Characteristics of Synapses Fixed while Uncoupled

Concomitantly with the increase in R_j resulting from axoplasmic acidification (Figs. 1 and 2), the synapses in the septum underwent substantial structural changes. Quantification of freeze-fracture replicas of axons fixed while uncoupled showed that the total number of gap junction plaques decreased from >3,000 for basal conditions to ~600 after sam-

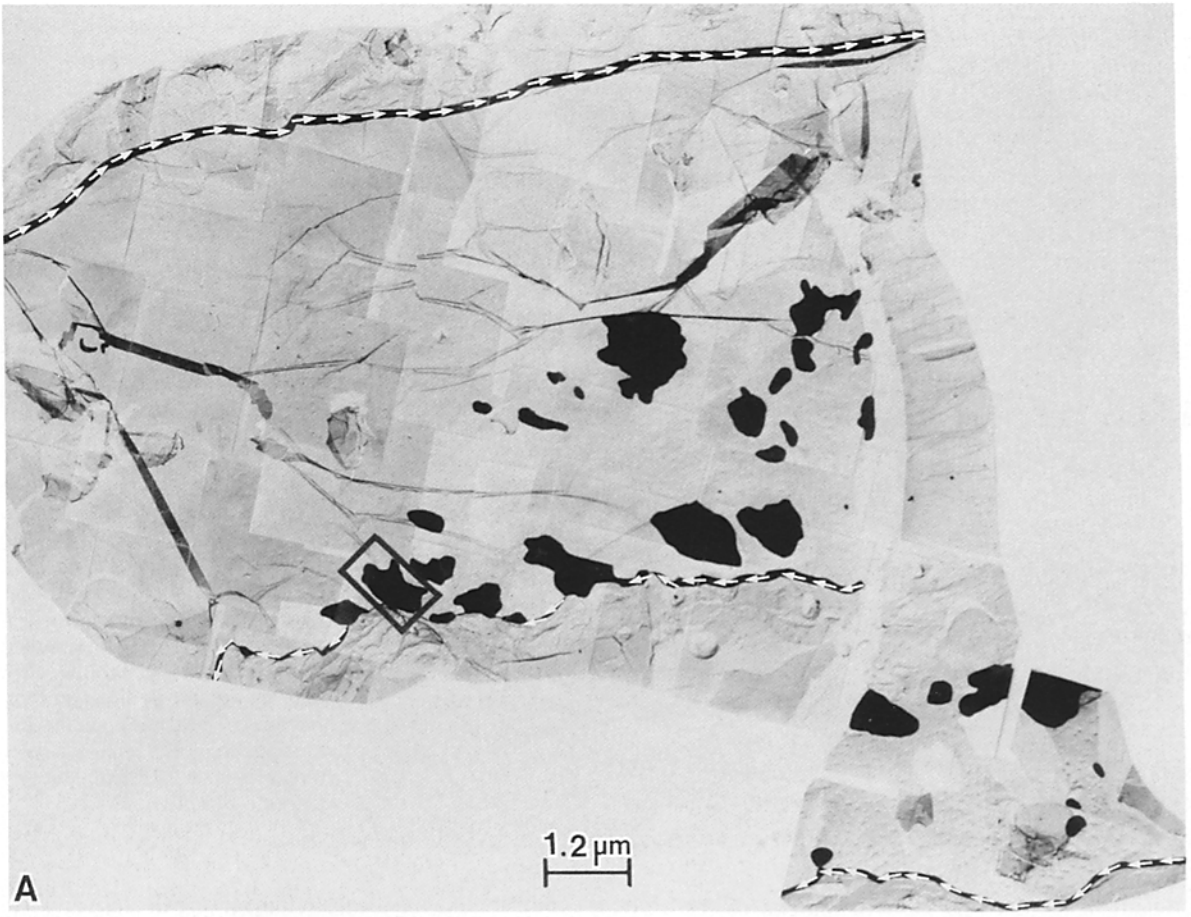
1.2 µm
A

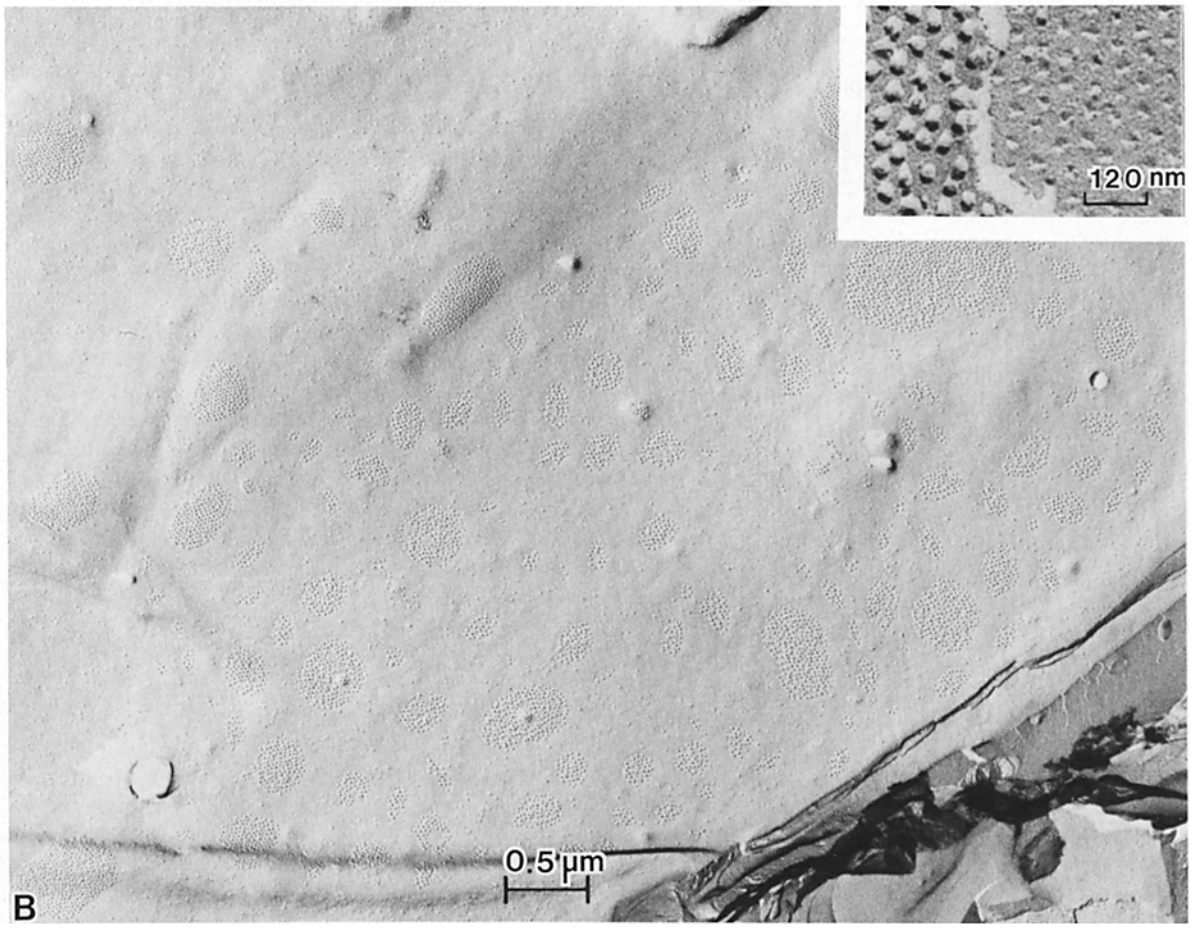
120 nm
0.5 µm
B

Table I. Quantification of Structural Parameters of Septa-connecting Crayfish Lateral Giant Axons Fixed in Basal Conditions (R_j = 60–80 kΩ) and Uncoupled Conditions ($R_j \approx$ 300 kΩ)

	Coupled	Uncoupled
Area of septum (μm^2)	2–3 × 10^4 (2)	–
Area of synapse (μm^2)	1.35 ± 0.4 × 10^3 (7)	1.6 ± 0.7 × 10^2 (9)
Area gap junction (μm^2)	1.3 ± 0.3 × 10^2 (7)	12 ± 2 (9)
Particle spacing (nm)	19.7 ± 1.6 [23]	20.1 ± 1.9 [18]
Diameter of particle (nm)	12 ± 0.9 [40]	11.7 ± 1.3 [50]
Number of particle	3.5 ± 0.2 × 10^5 (7)	3.1 ± 0.5 × 10^4 (9)
Number of vesicles	1.3–1.5 × 10^5 (5)	Decreased

The number in parenthesis corresponds to the number of freeze-fracture replicas analyzed covering at least 2,000 μm^2 of septa (each replica corresponds to a different septa). The numbers between brackets correspond to number of measurements given as mean ± SD. The number of particles and vesicles is per septum.

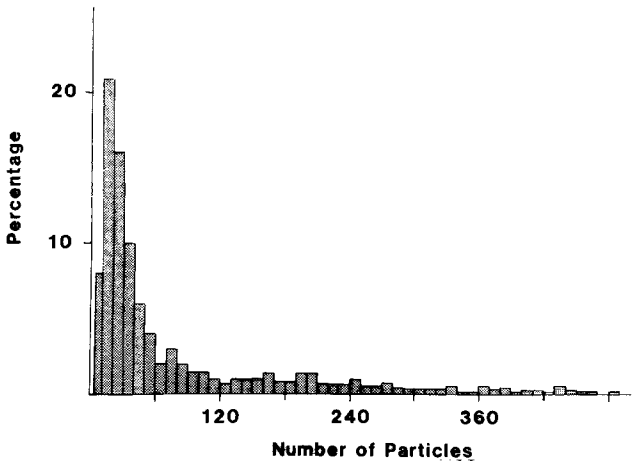

Figure 6. Histogram of the size distribution of gap junction plaques constructed from the analysis of 1,287 plaques obtained from synapses fixed in basal conditions. The abscissa represents the number of particles per plaque and the ordinate represents their percentage frequency of occurrence. Plaques containing over 500 particles occurred with small frequency and consequently were not shown. The first bar of the histogram included plaques containing between 6 and 10 particles and hence it is thinner than the others. A plaque was defined as an aggregate of six or more particles having center-to-center spacings of ~20 nm.

pling the same septal area (~28,000 μm^2). The synaptic area decreased from 1.35 ± 0.4 × 10^3 μm^2 in basal conditions to 1.6 ± 0.7 × 10^2 μm^2 (Table I). The number of particles in plaques decreased ~11-fold to 3.1 ± 0.5 × 10^4 (Table I). On the other hand, the frequency distribution of the number of particles per gap junction plaque, the diameter of the particles, and the center-to-center spacing of the particles in plaques remained as in basal conditions (compare Fig. 8, *A* and *B*). That is, upon uncoupling by axoplasmic acidification the morphology of the plaques remained unchanged. The two major structural modifications occurring during uncoupling by acidification were (*a*) the total number of particles in plaques (n_p) decreased by 90%, and (*b*) single junctional particles greatly increased in the nonjunctional axolemmae (Fig. 8, *A* and *B*).

Additional information regarding the structural organization of synapses fixed while uncoupled was obtained by thin sectioning. Synapses fixed after axoplasmic acidification contained segments of gap junctions (Fig. 9, *A* and *B*) characterized by transverse densities spaced 20 nm center-to-center apart, a 4–6-nm-wide gap, and associated vesicles (as in synapses fixed in basal conditions). However, the synapses fixed while uncoupled also exhibited other types of axolemmal specializations not present in basal conditions (compare Figs. 7 *B* and 9 *A*). These include regions where the axolemmae were separated by a much wider extracellular gap that lacked transverse densities (Fig. 9) and the presence of dense layers attached to the axolemma via slender projections (shown at higher magnification in Fig. 9 *C*). In these regions, coated pits (Fig. 9 *D*) and vesicles fused with the axolemma were observed (*large arrow*, Fig. 9, *A* and *C*). Another common feature of synapses fixed uncoupled was the presence of regions where the extracellular gap decreased to dimensions where it was barely resolved (region between the arrowheads in Fig. 9 *A*). Similar observation was reported by Peracchia and Dulhunty (31) in synapses uncoupled by bathing nerve cords in VH solution containing 0.5–5 mM 1,4-dinitrophenol.

The characteristic vesicles associated with synapses were also altered by axoplasmic acidification. The vesicles were no longer associated exclusively with the cytoplasmic surfaces of the synapses. Most vesicles remained free or formed clusters in the axoplasm. The regions of the junction devoided of vesicles also lacked transverse densities and the characteristic 4–6-nm-wide extracellular gap. In addition, the axoplasm of these synapses contained other membrane-bound organelles such as multivesicular bodies of irregular sizes and shapes containing vesicles (some of which were "coated"), tubular profiles, and flattened cisternae. All these structural changes show that large rearrangements of the synaptic regions occur during uncoupling by acidification.

Discussion

This study shows that the increase in junctional resistance, R_j, resulting from axoplasmic acidification was accompa-

Figure 5. (*A*) Montage of a freeze-fracture replica of a septal region that followed the E-face for ~7,000 μm^2 before deviating into the axoplasm. The dark lines with white arrows represent the points where the fracture plane jumped from the septum into the surrounding glial cells. The artificially blackened regions of the septum corresponded to the synapses (see *arrows* in Fig. 4). The synapse enclosed by the rectangle and pointed to by the arrow is presented at higher magnification in Fig. 5 *B*. (*B*) The synapse consists of gap junction plaques of different diameters and nonjunctional axolemmae. The inset shows a higher magnification of a junctional plaque displaying the E–P transition with particles on the E-face and complementary pits on the P-face.

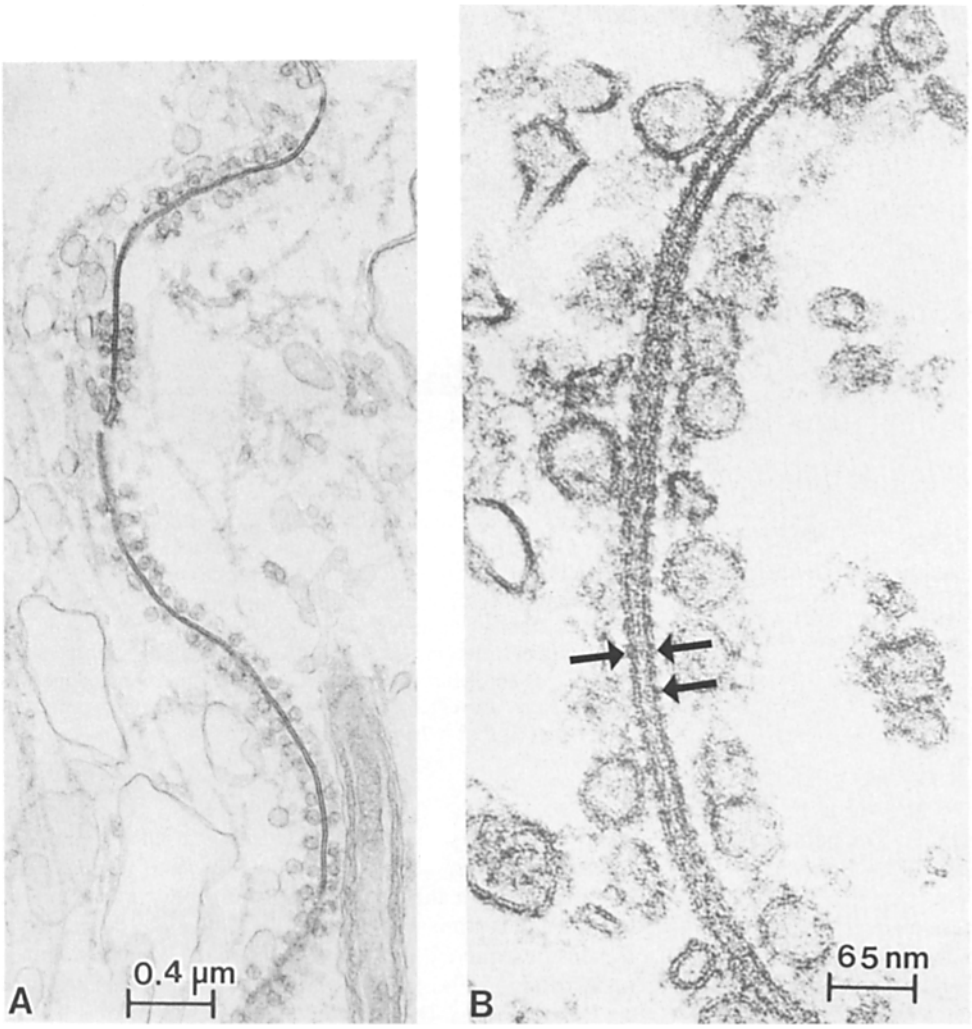

Figure 7. (*A*) Low magnification view of a region of axolemmal contact (synapse) fixed in basal conditions. The axolemmae are closely apposed through most of the synapse and vesicles are attached to both cytoplasmic surfaces. The axoplasms of both axons normally contain large vacuoles, mitochondria, and cytoskeletal elements. (*B*) Higher magnification view of a gap junction. The two axolemmae are separated by a small unstained gap and transverse densities (channels) span the membranes, bridge the extracellular gap, and protrude into the axoplasms.

nied by large structural rearrangements of the synaptic regions. These rearrangements included a decrease in the number of junctional particles in plaques (n_p) and an increase in the number of "single" gap junction particles in the axolemmae. These structural changes associated with uncoupling are different from those described by Peracchia and Dulhunty (31) in the same synapse. These authors reported that the main structural changes observed during uncoupling are decreases in both the diameter of the junctional particles (i.e., the channels) and their center-to-center spacing. In the present study, the comparison of gap junction plaques fixed in basal conditions and uncoupled showed that both the center-to-center spacing and the diameter of particles remained unchanged. These observations are consistent with structural studies of junctional uncoupling performed in other tissues (7, 22, 33). However, the failure to reproduce the observations of Peracchia and Dulhunty (31) could be attributed to the different experimental maneuvers used to uncouple these axons. We have used axoplasmic acidification by partial replacement of the external NaCl for Na acetate, whereas Peracchia and Dulhunty uncoupled the axons by the addition of DNP or EGTA to the external solution, compounds which are expected to change the internal calcium concentration. Therefore, the two studies might not be directly comparable and it may be that different uncoupling methods affect the normal structure of the synapses in different ways.

Crayfish gap junctions fracture differently than mammalian gap junctions leaving particles on the E-face and pits on the P-face (9, 28, 31). This characteristic, together with the fact that single junctional particles can be distinguished from regular intramembrane particles by their diameter and morphology, permits one to obtain the total number of gap junction particles in the synaptic regions (n_t = particles in plaques + single particles). Experiments in synapses fixed in basal conditions indicated that ~90% of the gap junction particles were aggregated in plaques ($n_t \approx n_p$). We will proceed to suggest that most of these junctional particles probably correspond to channels in the open state ($n_p \approx n_o$). This is accomplished by calculating the single channel conductance ($\delta_j = 1/[R_j \times n_o]$) from the experimental values of n_p (3.5×10^5) and R_j, and showing that this calculated value is similar to experimental values of δ_j obtained from whole cell patch clamp measurements (4, 24, 51). Measured values of junctional resistance depend on the distance between the recording electrodes and the septa. In crayfish septa, Johnston and Ramón (12) found that R_j is linearly related to the distance of the recording microelectrodes from the septa.

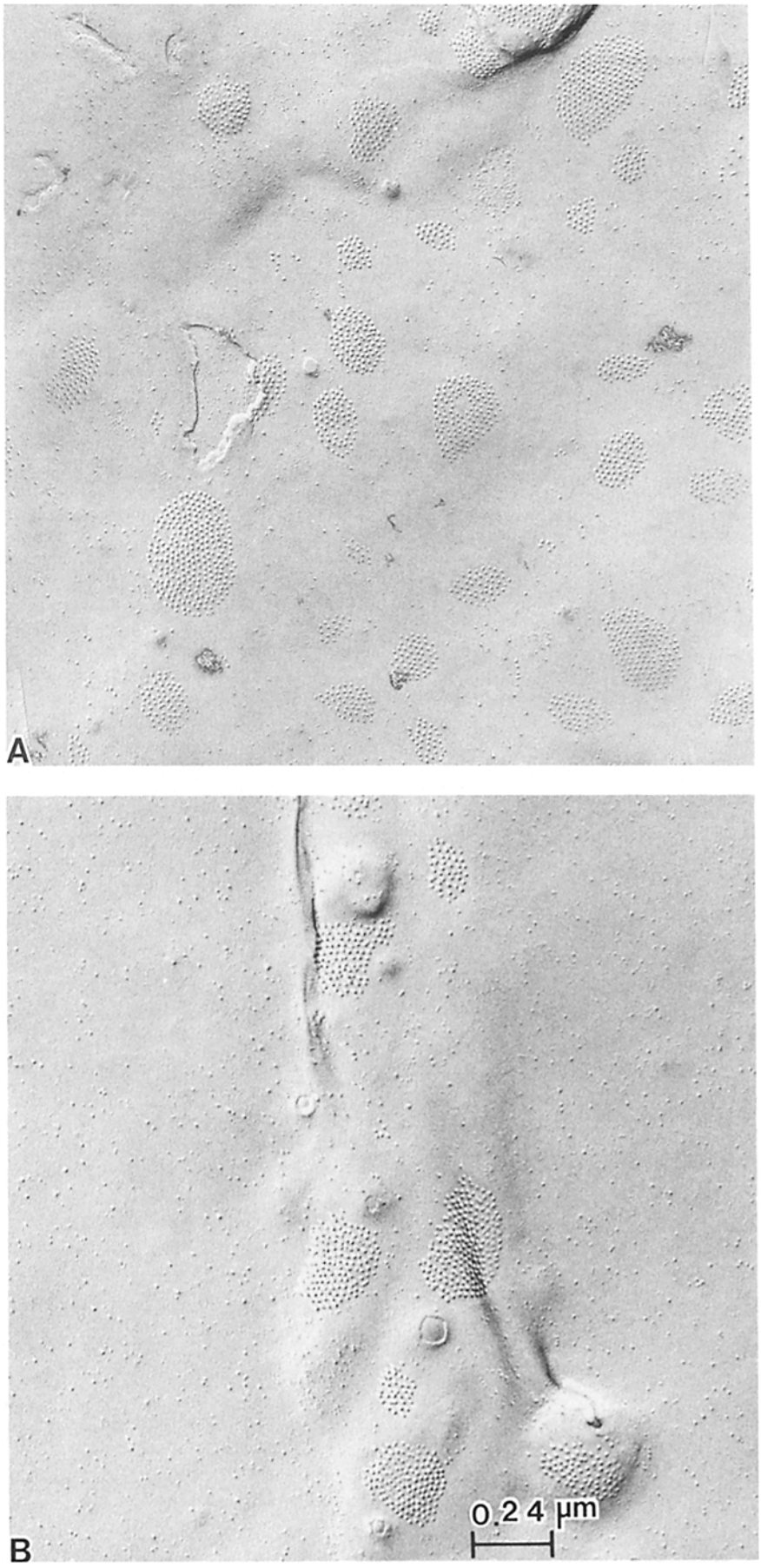

Figure 8. (*A*) Freeze-fracture replica of a synapse fixed in basal conditions displayed gap junction plaques and few single junctional particles. (*B*) Freeze-fracture replica of a synapses fixed uncoupled. The E-fracture face contains gap junction plaques and numerous "single" junctional particles. The frequency distribution, the diameter of the particles, and the center-to-center spacing of the gap junction plaques in uncoupled conditions was similar to the one described in Fig. 6. Both panels are presented at the same magnification, and the apparent differences were due to the local angle of shadowing, which is far more acute in the synapse fixed uncoupled.

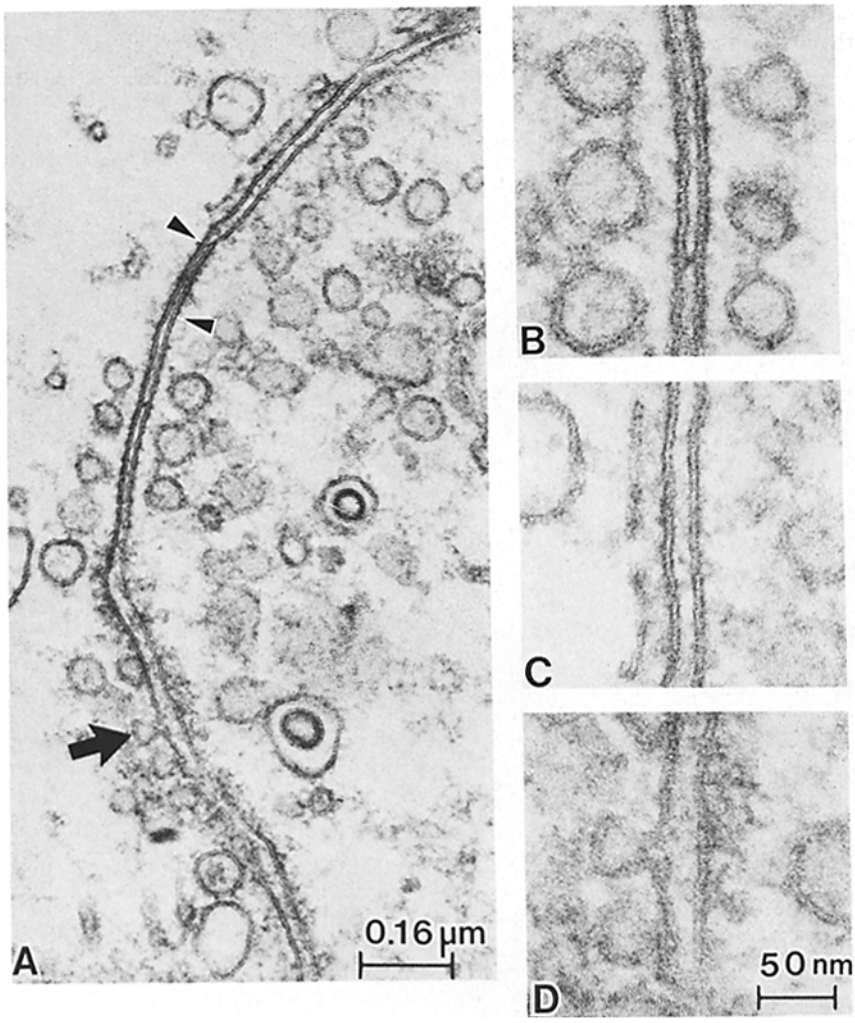

Figure 9. (*A*) Thin section electron microscopy of synapse fixed uncoupled. Note that (*a*) "typical" gap junctions are observed limited to smaller region of the synapse; (*b*) the synaptic vesicles were mostly free in the axoplasm; (*c*) the axolemmae were mostly separated by wider extracellular gaps (~10 nm in the region above the small gap junction and ~20 nm in the region below) devoid of transverse densities (compare with Fig. 7 *B*); (*d*) the extracellular gap can collapse (widths smaller than 4–6 nm) as shown in the region between the arrowheads. (*B–D*) Sectors of the synapse shown in *A* presented at higher magnification to illustrate the different types of axolemmal contact in the synapses fixed uncoupled. *B* shows a typical gap junction displaying most of their morphological characteristics (i.e., overall thickness, transverse densities, and associated vesicles). *C* shows the region above the arrowheads in *A* to demonstrate the increase in the width of the extracellular gap and a dense layer associated with one of the membranes. This layer may be involved in maintaining the vesicles associated exclusively to the junctional regions. *D* shows the region indicated by the arrow in *A*. Here the extracellular space was increased to ~20 nm wide and a vesicle is fused with the axolemma.

From this relationship they extrapolated to zero electrode distance and obtained a value of R_j of 16.6 kΩ (12). Using 16.6 kΩ for R_j and, assuming that all the particles in plaques ($n_p = 3.5 \times 10^5$) were open channels, a value of 170 pS was obtained for δ_j in basal conditions. This value is in good agreement with single channel conductances between pairs of cells (90–180 pS; 3, 21, 46) and in studies where gap junction proteins were reconstituted into planar lipid films (160–240 pS; 54, 58). Therefore, the assumption that, in basal conditions, most gap junction particles are in plaques and most of these particles are open channels appears justified (i.e., $n_t \approx n_p \approx n_o$).

Similar calculations were performed with data obtained after uncoupling by axoplasmic acidification to pH_i 6.7–6.8. At this pH_i, action potentials propagated in the axons but were blocked at the septal region. Unfortunately, acidification to pH_i 6.7–6.8 produced a range of R_j values (250–400 kΩ) which depended on factors such as the position of the electrodes with respect to the septum, time of the day at which the animals were sacrificed, and hormonal conditions of the animal (i.e., postmolt, intermolt, or premolt). For this calculation, the value of R_j used was 275 kΩ, the mean of 11 experiments. The same correction for the input resistance in basal conditions was used for uncoupled axons since R_1 and R_2 did not change appreciably when at pH_i 6.7–6.8 (275 − 50 = 225 kΩ). If again it is assumed that all the particles in plaques observed in the uncoupled axons (3.1×10^4) correspond to open channels, a value of 143 pS was obtained. Thus, considering the experimental uncertainties in the values of R_j and n_p, the calculated values of δ_j under basal and uncoupled conditions were not only in good agreement with each other but also within the range of values reported for gap junction channels between other cells.

The above analysis suggests that when channels are in plaques the probability of them being open is greater than their probability of being closed. This conclusion is difficult to test experimentally because single channel recordings between cell pairs do not provide direct information about the total number of channels in the region of contact nor whether they exist aggregated in plaques or single. Moreover, values for the probability of the gap junction channel being open seems to vary for different tissues. For example, in single channel recordings between embryonic muscle cell pairs this probability is ≤ 0.9 (4). Similarly, recordings between lacrimal cell pairs (24) suggest that the channels spend more time in the open than in the closed state. In contrast, studies in isolated cardiac cells (51) show that the probability for the channel being open is 0.16. Therefore, it appears that one of

the properties of the channel, the mean open time, depends on the type of cell being studied and perhaps on the experimental conditions.

That the number of particles in plaques (n_p) is closely related to the number of open channels (n_o) has two important consequences. One is that action potentials will fail to propagate across the septa when 90% of the particles are dispersed into the axolemmae either as closed channels or as hemi-channels. Therefore, the excess of gap junction channels present in basal conditions may represent a safety factor in the escape reflex of the animal. The other consequence is that the number of open channels (in plaques) when R_j reaches 1.3 MΩ (Fig. 2) was calculated to be 4.5×10^3. This calculation suggests that, from the value of R_j at which the septa fail to propagate action potentials (250–400 kΩ) to its maximum value (1.3 MΩ), only 8–10% of the total number of channels need to close.

These results also suggest that junctional particles in plaques become dispersed upon acidification. Dispersion of junctional particles has been previously reported to occur upon uncoupling by cytoplasmic acidification in other cells (15, 17). Thus, dispersion may be part of the normal mechanism for gap junction channel renewal. These single gap junctional particles resulting from dispersion from plaques could correspond to closed channels or hemichannels. Thin sections of synapses fixed while uncoupled demonstrated that the width of the extracellular gap increased to 10–20 nm upon axoplasmic acidification and that transverse densities were absent from these regions (Fig. 8). Therefore, it seems likely that the dispersed single particles represent hemichannels because their extracellular domains cannot span such large gaps.

The presence of coated vesicles, coated pits, and primary and secondary lysosmes strongly suggests that during uncoupling by acidification, components of the synapse are being internalized by mechanisms similar to those described in receptor-mediated endocytosis (41).

We wish to thank Drs. A. Rivera, E. Bosch, and R. Arellano for helpful comments on the original manuscript.

This work was supported by grants EY04110 and NS20669 from the National Institutes of Health. We also acknowledge support from the Muscular Dystrophy Associations of America through the Jerry Lewis Neuromuscular Research Center Grant. A. L. Moreno was supported by a fellowship from CONACyT, Mexico.

Received for publication 23 March 1987, and in revised form 22 December 1987.

References

1. Arellano, R. O., R. Ramón, A. Rivera, and G. Zampighi. 1986. Lowering of pH does not directly affect the junctional resistance of crayfish lateral axons. *J. Membr. Biol.* 94:293–299.
2. Benedetti, E. L., and P. Emmelot. 1968. Hexagonal arrays of subunits in tight junctions separated from isolated rat liver plasma membranes. *J. Cell Biol.* 38:15–24.
3. Campos de Carvalho, A., D. C. Spray, and M. V. L. Bennett. 1984. pH dependence of transmission st electrotonic synapse of the crayfish septate axon. *Brain Res.* 321:279–286.
4. Chow, I., and S. H. Young. 1987. Opening of single gap junction channels during formation of gap junction channels between embryonic muscle cells. *Dev. Biol.* 122:332–337.
5. Flagg-Newton, J. L., G. Dahl, and W. R. Loewenstein. 1981. Cell junction and cyclic AMP. I. Upregulation of junctional membrane permeability and junctional membrane particles by administration of cyclic nucleotides or phosphodiesterase inhibitor. *J. Membr. Biol.* 63:105–121.
6. Flower, N. E. 1972. A new junctional structure in the epithelia of insecta of the order Dictyoptera. *J. Cell Sci.* 10:683–691.
7. Green, C. R., and N. J. Severs. 1984. Gap junction connexon configuration in rapidly frozen myocardium and isolated intercalated disks. *J. Cell Biol.* 99:453–463.
8. Hama, K. 1961. Some observations on the fine structure of crayfishes (*Cambarus virilis* and *Cambarus clarkii*) with special reference to the organization of the synapses. *Anat. Rec.* 141:275–293.
9. Hanna, R. B., G. D. Pappas, and M. V. L. Bennett. 1984. The fine structure of identified electrotonic synapses following increase coupling resistance. *Cell Tiss. Res.* 235:243–249.
10. Hax, W. M. A., G. E. P. Venrooij, and J. B. Vossenberg. 1974. Cell communication: a cyclic-AMP mediated phenomenon. *J. Membr. Biol.* 19: 253–266.
11. Johnson, G. A. 1924. Giant nerve fibers in crustaceans with special reference to *Cambarus* and *Paleomonetes*. *J. Comp. Neurol.* 36:323–373.
12. Johnston, M. F., and F. Ramón. 1981. Electrotonic coupling in internally perfused crayfish segmented axons. *J. Physiol. (Lond.).* 317:509–518.
13. Johnston, M. F., S. A. Simon, and F. Ramón. 1980. Interaction of anesthetics with electrical synapses. *Nature (Lond.).* 286:498–500.
14. Kramer, A. P., F. B. Krasne, and J. J. Wine. 1981. Interneurons between giant axons and motoneurons in crayfish escape circuitry. *J. Neurophysiol. (Bethesda).* 45:550–573.
15. Lane, N. J., and L. S. Swales. 1980. Dispersal of particles, not internalization, during the in vivo disappearance of gap junctions. *Cell.* 19:579–586.
16. Lasater, E. M., and J. E. Dowling. 1985. Electrical coupling between pairs of isolated fish horizontal cells is modulated by Dopamine and cAMP. *In* Gap Junctions. M. V. L. Bennett and D. C. Spray, editors. Cold Spring Harbor Laboratory, NY. 393–404.
17. Lee, W. M., D. G. Cran, and N. J. Lane. 1982. Carbon dioxide induced disassembly of gap junctional plaques. *J. Cell Sci.* 57:215–228.
18. Loewenstein, W. R. 1966. Permeability of membrane junctions. *Ann. N.Y. Acad. Sci.* 137:441–472.
19. Loewenstein, W. R. 1981. Junctional intercellular communication. The cell-to-cell membrane channel. *Physiol. Rev.* 61:829–913.
20. Makowsky, L., D. L. D. Caspar, W. C. Phillips, D. A. Goodenough. 1977. Gap junction structures. II. Analysis of the x-ray diffraction data. *J. Cell Biol.* 74:629–645.
21. McNutt, N. S., and R. S. Weinstein. 1970. The structure of the nexus. A correlated thin section and freeze-cleaved study. *J. Cell Biol.* 47:666–688.
22. Miller, T. M., and D. A. Goodenough. 1985. Gap junction structures after experimental alteration of junctional channel conductance. *J. Cell Biol.* 101:1741–1748.
23. Moreno, A. P., F. Ramon, and D. C. Spray. 1987. Variation of gap junction sensitivity to H-ions with time of the day. *Brain Res.* 400:181–184.
24. Neyton, J., and A. Trautmann. 1985. Single-channel currents of an intercellular junction. *Nature (Lond.).* 317:331–335.
25. Obaid, A. L., S. J. Socolar, and B. Rose. 1983. Cell-to-cell channels with two independent regulated gates in series: analysis of junctional conductance modulation by membrane potential, calcium, and pH. *J. Membr. Biol.* 73:69–89.
26. Pappas, G. D., Y. Asada, and M. V. L. Bennett. 1971. Morphological correlates of increased coupling resistance at an electrotonic synapse. *J. Cell Biol.* 49:173–188.
27. Peracchia, C. 1973. Low resistance junctions in crayfish. I. Two arrays of globules in junctional membranes. *J. Cell Biol.* 57:54–65.
28. Peracchia, C. 1973. Low resistance junctions in crayfish. II. Structural details and further evidence for intercellular channels by freeze-fracture and negative staining. *J. Cell Biol.* 57:66–76.
29. Peracchia, C. 1984. Communicating junctions and calmodulin: inhibition of electrical uncoupling of Xenopus embryo by calmidazolium. *J. Membr. Biol.* 81:49–58.
30. Peracchia, C. 1987. Calmodulin-like proteins and communicating junctions. Electrical uncoupling of crayfish septate axons is inhibited by calmodulin inhibitor W7 and is not affected by cyclic nucleotides. *Pfluegers Arch. Eur. J. Physiol.* 408:379–385.
31. Peracchia, C., and A. F. Dulhunty. 1976. Low resistance junctions in crayfish. Structural changes with functional uncoupling. *J. Cell Biol.* 70:419–439.
32. Ramón, F., and G. Zampighi. 1980. On the electrotonic coupling mechanism of crayfish segmented axons. Temperature dependence of junctional conductance. *J. Membr. Biol.* 54:165–171.
33. Raviola, E., D. A. Goodenough, and G. Raviola. 1980. Structure of rapidly frozen gap junctions. *J. Cell Biol.* 87:273–279.
34. Revel, J. P., and M. J. Karnovsky. 1967. Hexagonal array of subunits in intercellular junctions of the mouse heart and liver. *J. Cell Biol.* 33: C7–C12.
35. Robertson, J. D. 1953. Ultrastructure of two invertebrate synapses. *Soc. Exp. Biol. Med.* 82:219–223.
36. Robertson, J. D. 1954. Electron microscope study of an invertebrate synapse. *Fed. Proc.* 13:119.
37. Robertson, J. D. 1955. Recent electron microscopic observations on the ultrastructure of a crayfish median-to-motor giant synapse. *Exp. Cell Res.* 8:226–229.
38. Robertson, J. D. 1963. The presence of a subunit pattern in the unit mem-

brane of club endings in Mauthner cell synapses in goldfish brain. *J. Cell Biol.* 19:201–221.
39. Rose, B., and W. R. Loewenstein. 1975. Permeability of cell junction depends on local cytoplasmic calcium activity. *Nature (Lond.).* 254:250–252.
40. Saez, J. C., D. C. Spray, A. C. Nairn, E. Hertzberg, P. Greengard, and M. V. L. Bennett. 1986. cAMP increases junctional conductance and stimulates phosphorylation of the 27 kDa principal gap junction polypeptide. *Proc. Natl. Acad. Sci.* 83:2473–2477.
41. Sibley, D. R., and R. J. Lefkowitz. 1985. Molecular mechanism of receptor desensitization using the β-adrenergic receptor-coupled adenylate cyclase system as a model. *Nature (Lond.).* 317:124–129.
42. Spray, D. C., and M. V. L. Bennett. 1985. Physiology and pharmacology of gap junctions. *Annu. Rev. Physiol.* 47:281–303.
43. Spray, D. C., A. L. Harris, and M. V. L. Bennett. 1979. Voltage dependence of junctional conductance in early amphibian embryos. *Science (Wash. DC).* 204:432–434.
44. Spray, D. C., A. L. Harris, and M. V. L. Bennett. 1981. Equilibrium properties of a voltage-dependent junctional conductance. *J. Gen. Physiol.* 77:77–93.
45. Spray, D. C., A. L. Harris, and M. V. L. Bennett. 1981. Gap junction conductance is a simple and sensitive function of intracellular pH. *Science (Wash. DC).* 211:712–715.
46. Turin, L., and A. Warner. 1977. Carbon dioxide reversible abolishes ionic communication between cells of early amphibian embryo. *Nature (Lond.).* 270:56–57.
47. Turin, L., and A. Warner. 1980. Intracellular pH in early Xenopus embryos: its effect on current flow between blastomeres. *J. Physiol. (Lond.).* 300:489–504.
48. Unwin, P. N. T., and P. D. Ennis. 1983. Calcium-mediated changes in gap junction structure: evidence from low-angle x-ray pattern. *J. Cell Biol.* 97:1459–1466.
49. Unwin, P. N. T., and P. D. Ennis. 1984. Two conformation of a channel forming protein. *Nature (Lond.).* 307:609–613.
50. Unwin, P. N. T., and G. Zampighi. 1980. Structure of junctions between communicating cells. *Nature (Lond.).* 283:545–549.
51. Veenstra, R. D., and R. L. De Haan. 1986. Measurement of single channel currents from cardiac gap junctions. *Science (Wash. DC).* 233:972–974.
52. Watanabe, A., and H. Grundfest. 1961. Impulse propagation at the septal and commisural junctions of crayfish lateral axons. *J. Gen. Physiol.* 45:267–308.
53. Yada, T., B. Rose, and W. R. Loewenstein. 1985. Diacylglycerol downregulates junctional membrane permeability. TMB-8 blocks its effect. *J. Membr. Biol.* 88:217–232.
54. Young, D-E. J., Z. A. Cohn, and N. B. Gilula. 1987. Functional assembly of gap junction conductance in lipid bilayers: demonstration that the major 27 kd proteins forms the junctional channel. *Cell.* 48:733–743.
55. Zampighi, G. 1980. On the structure of isolated junction between communicating junctions. *In Vitro. (Rockville).* 16:1018–1028.
56. Zampighi, G., and P. N. T. Unwin. 1979. Two forms of isolated gap junctions. *J. Mol. Biol.* 135:451–464.
57. Zampighi, G., J. M. Corless, and J. D. Robertson. 1980. On gap junction structure. *J. Cell Biol.* 86:190–198.
58. Zampighi, G., J. E. Hall, and M. Kreman. 1985. Purified lens junctional protein forms channels in planar lipid films. *Proc. Natl. Acad. Sci. USA.* 82:8468–8472.
59. Zampighi, G., F. Ramón, and W. Durán. 1978. Fine structure of the electrotonic synapses of the lateral axons in a crayfish (*Procambarus clarkii*). *Tissue & Cell.* 10:413–426.